J. Plasma Fusion Res. SERIES, Vol. 9 (2010)

Alfvén wave propagation in initial value MHD simulation in a tokamak geometry

Y. Nishimura and C. Z. Cheng

Plasma and Space Science Center, National Cheng Kung University, Tainan 70101, Taiwan

(Received: 30 October 2009 / Accepted: 10 February 2010)

Alfvén wave propagation in an initial value magnetohydrodynamic (MHD) simulation is reported. The simulation result is compared with the theoretical shear Alfvén wave dispersion relation both in a cylindrical geometry and in a toroidal geometry. Generation of the toroidicity induced Alfvén eigenmode (TAE) frequency gap is observed in the presence of 1/R variation of the toroidal magnetic field. As a preliminary test, excitation of TAE mode is simulated in the presence of energetic particles. A numerical scheme employed in the simulation (the second order moment of the kinetic ions and electrons from particle simulation replace the pressure evolution equation) is discussed.

Keywords: Toroidicity induced Alfvén eigenmode, kinetic-fluid model, MHD simulation, gyrokinetic theory, particle simulation

1. Introduction

Energetic particles can play important roles in burning plasmas. For example, Toroidicity induced Alfvén Eigenmodes (TAE)[1, 2] can be excited when energetic particles (e.g. fusion born alpha particles),[3, 4] resonate with the phase velocity of the shear Alfvén wave within the frequency gap of the Alfvén continuum. Another example where the energetic particles play important roles is the stabilization of sawtooth oscillations.[5, 6, 7] Long period sawteeth accompanying the Alfvénic instabilities are reported. In this work, employing a kinetic-fluid simulation model,[8] the Alfvénic instabilities are studied in tokamak plasmas. The kinetic-fluid model incorporates all the particle dynamics through the pressure tensor by taking the second order moment of the particle simulation while the electromagnetic field quantities are evolved in the fluid equations.[8] The kinetic-fluid model retains the ion and electron wave-particle interaction for both the bulk and the energetic particle components. The model allows to study the interaction of the energetic particles with thermal kinetic ions and electrons in contrast to the conventional kinetic-MHD hybrid models.[9, 10, 11, 12, 13] The advantage of initial value approach is its application for nonlinear simulation (and for studying resonant type instabilities such as RTAE).[14, 15] Our final goal is to examine the saturation mechanism of the instabilities incorporating geometrical effects correctly. We approach step by step toward our long term goal. We start from examining global Alfvén oscillation, continuum damping, and the generation of the TAE gap in the toroidal geometry due to the magnetic field inhomogeneity (in the MHD limit). We then incorporate kinetic energetic particles to excite the instabilities. In Sec. 2 the basic model for MHD simulation is discussed. Section 3 presents simulation results. We summarize this work in Sec. 4.

author's e-mail: nishimura@pssc.ncku.edu.tw

2. Basic model for computation

A nonorthogonal, straight-field-line coordinate system is employed in the present calculations, in which ρ is the flux surface label, θ is the poloidal-like angle, and ζ is the toroidal angle. The magnetic field in a tokamak is given by

$$\mathbf{B} = \mathbf{B_{eq}} + \tilde{\mathbf{B}}, \tag{1}$$

$$\mathbf{B_{eq}} = \nabla\psi_{eq} \times (q\nabla\theta - \nabla\zeta), \tag{2}$$

$$\tilde{\mathbf{B}} \equiv \nabla \times \tilde{\mathbf{A}} = \nabla \times (-\psi\nabla\zeta) = \nabla\zeta \times \nabla\psi, \tag{3}$$

where $\psi_{eq}(\rho)$ stands for the equilibrium poloidal magnetic flux and equilibrium poloidal current. Here, $\psi(\rho,\theta,\zeta) = \sum_{m/n} \psi_{m/n}(\rho)\cos(m\theta + n\zeta)$ is the poloidal flux function of the perturbed field, where m and n are the poloidal and the toroidal mode numbers, respectively. We denote the total poloidal magnetic flux as $\psi_t(\rho,\theta,\zeta) \equiv \psi_{eq}(\rho) + \psi(\rho,\theta,\zeta)$.

Numerical simulation has been conducted employing a reduced MHD formulation[16] which allows simulating both cylindrical and toroidal geometries. Toroidal geometry can enter the set of equations via metric elements obtained from an equilibrium solver.[17] The initial value simulation is conducted by employing the FAR code.[18, 19] In our study the reduced MHD equations[16] are solved for the magnetic flux ψ, the toroidal component of the vorticity U^ζ, and the pressure P. The relevant equations are: the toroidal component of ideal Ohm's Law,

$$\frac{\partial\psi}{\partial t} = -R^2 (\mathbf{v} \times \mathbf{B}) \cdot \nabla\zeta, \tag{4}$$

the vorticity equation,

$$\rho_m \frac{dU^\zeta}{dt} = \frac{1}{c} R^2 \mathbf{B} \cdot \nabla J^\zeta + \left(\nabla R^2 \times \nabla P\right) \cdot \nabla\zeta, \tag{5}$$

In these equations, R stands for the major radius, $\mathbf{v} \equiv R^2\nabla\zeta \times \nabla\phi$ is the fluid velocity $[\phi(\rho,\theta,\zeta) = \sum_{m/n}\phi_{m/n}(\rho)\sin(m\theta+n\zeta)$ is the stream function$]$, $\mathbf{U} \equiv \nabla\times(R^2\mathbf{v})$ is the vorticity, and $\mathbf{J} = (c/4\pi)\nabla\times\mathbf{B}$ is the current density. The mass density is given by ρ_m (we assume plasma to be incompressible and thus ρ_m is constant in this paper). Superscripts denote the contravariant components.

In the momentum balance (the vorticity equation), the pressure is given by

$$\mathbf{P} = P_\perp(\mathbf{I} - \mathbf{bb}) + P_\parallel \mathbf{bb} \tag{6}$$

(the off diagonal tensor element is ignored for the moment)

$$P_{\perp j} = \int \mu B \delta f_j d^3v, \tag{7}$$

$$P_{\parallel j} = \int m_j v_\parallel^2 \delta f_j d^3v. \tag{8}$$

which is obtained by taking second order moment of the particle simulation. Here, $\mathbf{I}$ is the identity matrix and $\mathbf{b} = \mathbf{B}/|B|$ is the unit vector along the magnetic field line. Toroidal curvature effects are included in the second term of Eq. (5). As suggested in Eqs. (7) and (8), the second order moment of the kinetic particles from particle simulation replace the pressure evolution equation. In Eqs. (7) and (8), the subscript j stands for the particle species.

The MHD simulation in this study is based on up-down symmetry of the equilibrium. Given a sine function as an initial condition for the stream function ϕ, the sine terms in ψ and the cosine terms in ϕ remain zero.[20] In the same manner the kinetic pressure retains a parity of cosine.

The kinetic ions and electrons are given by gyrokinetic δf Vlasov equation[21]

$$\frac{\partial \delta f_j}{\partial t} = -\dot{\mathbf{X}}\cdot\nabla f_0 - \dot{v_\parallel}\frac{\partial f_0}{\partial v_\parallel}. \tag{9}$$

The particle positions are time advanced using a second order Runge-Kutta-Gill method.[22]

$$\dot{\mathbf{X}} = v_\parallel \frac{\mathbf{B}^\star}{B_\parallel^\star} + \frac{c}{q_j B_\parallel^\star}\mathbf{b}\times(\mu\nabla B - q_j\mathbf{E}^\star) \tag{10}$$

$$\dot{v_\parallel} = -\frac{\mathbf{B}^\star}{m_j B_\parallel^\star}\cdot(\mu\nabla B - q_j\mathbf{E}^\star) \tag{11}$$

where $\mathbf{X}$ is the position, $v_\parallel$ is the velocity parallel to the equilibrium magnetic field, $\mu = m{v_\perp}^2/2B$ is the magnetic moment. Here, q_j is the charge of the particles and c is the speed of light. For the field quantities, $\mathbf{B}^\star = \mathbf{B} + \nabla\times(cm_jv_\parallel/q_j)\,\mathbf{b}$, and $\mathbf{E}^\star = -\nabla\phi - c^{-1}\partial_t\tilde{A}$. Note that the $\mathbf{B}^\star$ component contains the conventional curvature drift term. Here, $B_\parallel^\star = \mathbf{b}\cdot\mathbf{B}^\star$.

In the δf simulation, the weight equation[23] carries the information of the perturbed field (while the trajectories are unperturbed ones for the linear simulation). As an initial test we provide the simulation with only passing particles (we set $\mu = 0$ to avoid complications such as particles lost at the plasma boundary).

We incorporate the electron inertia term, the Hall term, and the gyroviscous term into the Ohm's law, as manifested in Ref.[8]. In this paper, however, we focus on incorporating the pressure closure relation Eqs. (7) and (8).

3. Simulation results in the MHD limit

Parameters used in the calculations are as follows. The q-profile (the safety factor) is taken as parabolic $q = 1.0 + \rho^2$. The equilibrium pressure profile has the form of $P = \psi_{eq}^2$. Major radius is given by $R = 5\ m$ and the minor radius $a = 1.25\ m$ (thus the inverse aspect ratio $\epsilon = 1/4$). A total of 200 equally spaced mesh points was used in the radial direction. The mode spectrum was selected as $m/n = 1/1$ and $m/n = 2/1$. Equations (4) and (5) are dissipationless. The resistivity and the viscosity terms[19] are set to be zero. In Eqs.(4) and (5), we provide ϕ with an initial perturbation of a sine parity.[20]

In Fig.1 (a), shear Alfvén wave oscillation is tested in a cylindrical limit. We set $R = 1$ in Eqs.(4) and (5). In Fig.1, single Fourier mode of $m = 1$ and $n = 1$ is taken. Here, time is normalized by $\omega_A = v_A/q_0R_0$ which is the Alfvén frequency at the magnetic axis ($q_0 = 1.0$ is the safety factor and R_0 is the major radius at the magnetic axis, respectively). The wave equation (hyperbolic equation) and thus the shear Alfvén wave dispersion relation can be obtained by Eqs.(4) and (5) in the absence of the curvature driven term. The Alfvén wave frequency measured at different radial locations satisfies shear Alfvén wave dispersion relation $\omega = v_Ak_\parallel(\rho)$, where $k_\parallel = \rho^2/(1+\rho^2)$ which is plotted onto Fig.1(b).

Figure 2 shows the shear Alfvén wave frequency as a function of the radial coordinate ρ which is equivalent to Fig.1 of Ref.[4]. Due to the $1/R$ variation of the toroidal magnetic field (R is the major radius), the cylindrical Alfvén continuum (dashed lines) breaks up and the frequency gap (or the frequency forbidden band) appears within the range of $0.308 < \omega/\omega_A < 0.366$.

For the simulation in the toroidal geometry, the numerical equilibrium from a Grad-Shafranov solver[17] is employed. In Fig.3, shear Alfvén wave oscillation is tested in a toroidal geometry in the absence of kinetic particles [the dynamical pressure term in Eq.(5) is absent]. In Fig.3 (a), the $m = 1$ and the $m = 2$ oscillations are synchronized each other and

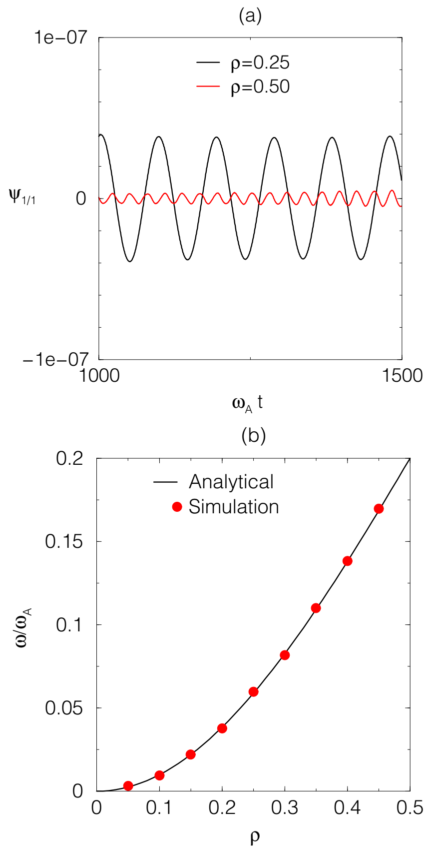

Fig. 1 Alfvén wave propagation in a cylindrical limit : (a) shear Alfvén wave oscillation (of the perturbed flux function ψ) at $\rho = 0.25$ and $\rho = 0.50$, (b) frequency versus the radial location. Frequencies from the simulation results match with the analytical prediction.

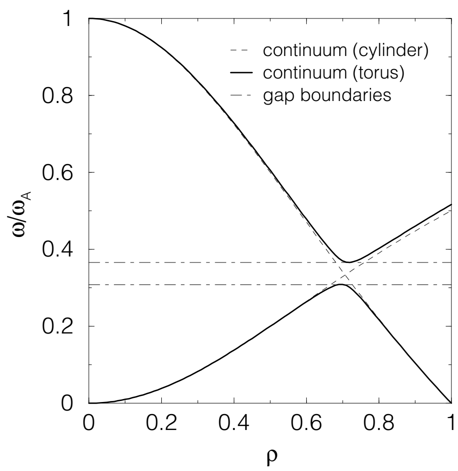

Fig. 2 Shear Alfvén frequency as a function of the radial location. The dashed curves are the continuum frequencies for the cylindrical limit, for $m = 1$ and $m = 2$ modes. The solid lines are the continuum frequency with the toroidal geometry effect. The lower (upper) boundary of the upper (lower) curve is at $\omega/\omega_A = 0.366$ ($\omega/\omega_A = 0.308$). The figure is a recapitulation of Fig.1 of Ref.[4].

behave as one global mode.

The frequency spectrum in Fig.3(b) is obtained by a Fourier transform of the time series in Fig.3(a). In Fig.3 (b), we find the frequency peak at one of the TAE gap boundaries (the lower boundary). In Fig.3 (c), the eigenmode of perturbed flux function ψ at three different incidents are plotted, which reveals a purely oscillatory behavior. These are good evidences that the Alfvén wave in our simulation is responding correctly to the toroidal geometry (and thus TAE).

In Fig.4, we show our preliminary simulation results incorporating Eqs.(7)-(11). We *push* energetic particles. The TAE mode is excited in the presence of energetic particle ions. The energetic particles are given by Gaussian distribution with the thermal velocity set to the Alfvén velocity. Here, $\beta_\alpha = 4\pi p_\alpha / B_0^2 = 0.01$ is taken (p_α is the pressure of the energetic particles). With the β_α value and assuming the equilibrium ion density to be $10^{20} m^{-3}$, the Larmor radius of a deuterium energetic particle at the Alfvén velocity is given by 1.82% of the minor radius. In this work, the background density gradient is parametrized by $a\,(\partial_\rho \log n_{eq}) = -1.0$. Here, n_{eq} is the equilibrium density profile. The mode amplitude of the ψ fluctuation experiences an exponential growth of the envelope together with the oscillation at the TAE frequency. The linear growth rate is given by $\gamma/\omega_A = 0.0027$ while the frequency is given by $\omega/\omega_A = 0.316$. In Fig.4(b), the frequency peak resides within the TAE gap. Figure 4(c) shows the TAE eigenmode structure in the presence of the energetic particles.

4. Summary and Discussions

In this work, we have discussed Alfvén wave propagation in cylindrical and toroidal geometries. We have observed the mode frequencies at the TAE gap in a toroidal geometry. Compared to the majority of the MHD simulation work[9, 10, 11, 12, 13, 18, 19] which have focused on the instability with finite dissipation in the system, the present work is unique in that it reveals the Alfvén oscillation in an ideal MHD limit (and by an initial value approach). Furthermore, linear excitation of TAE mode is demonstrated in the presence of energetic particles.

The advantage of the initial value approach is its application for nonlinear simulation. The kinetic-fluid model[8] can be a useful tool to study nonlinear saturation mechanism of Alfvénic instabilities. To conserve energy in the nonlinear simulation, we need to describe the the equilibrium distribution function in terms of invariant canonical flux surfaces.[24, 25]

We recapitulate the limitations given in the present paper. For the kinetic simulation, we did not incorporate particle drifts (we set $\mu = 0$) nor finite

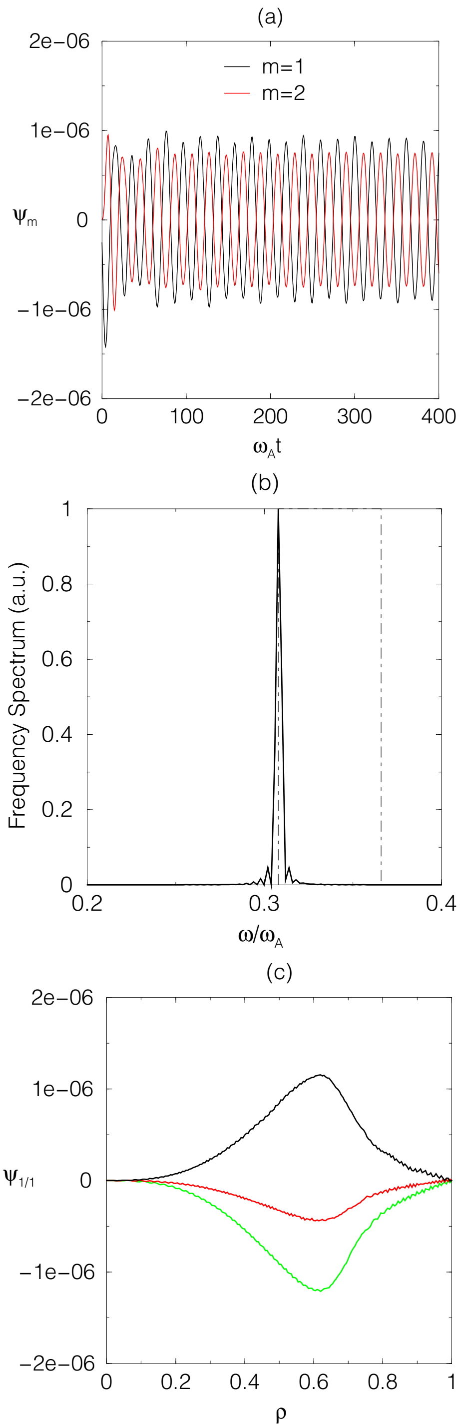

Fig. 3 (a) The Fourier components of the magnetic perturbation ψ as a function of time. (b) The frequency spectrum obtained from the time series of Fig.3(a). The peak is found at one of the boundary of the gap, $\omega/\omega_A = 0.308$. (c) the TAE eigenmode structure in the absence of drive, which goes through pure oscillation with time.

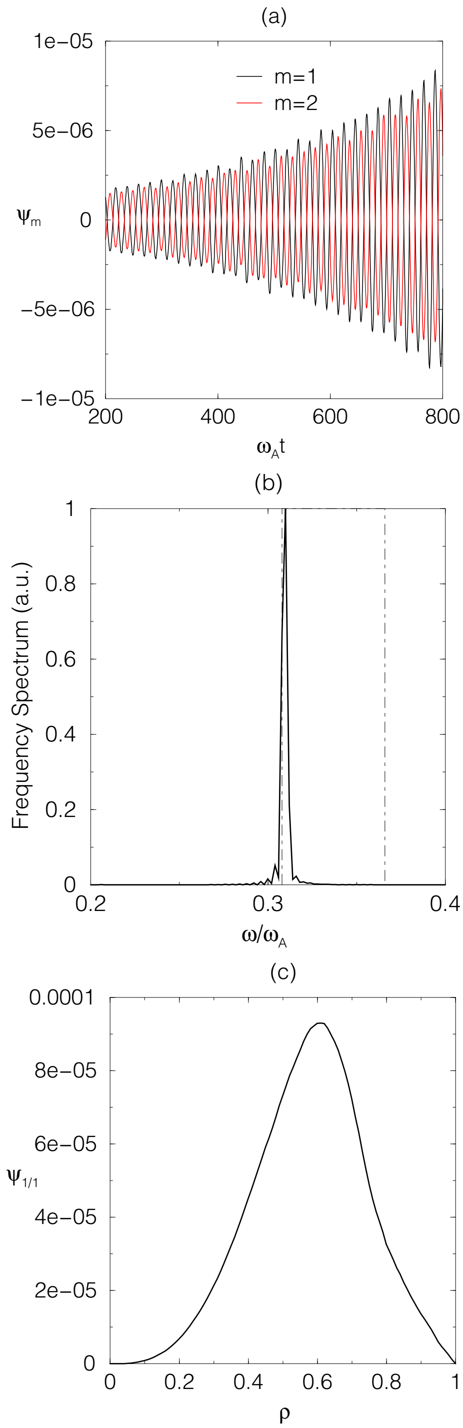

Fig. 4 (a) The Fourier components of the magnetic perturbation ψ as a function of time. (b) The frequency spectrum obtained from the time series of Fig.4(a), (c) the TAE eigenmode structure of $\psi_{1/1}$ in the presence of energetic particles.

Larmor radius effects. The thermal ions and electrons are absent as well (in the present paper).

This work is supported by National Cheng Kung University Top University Project. The authors would like to thank Dr.K. C. Shaing for useful discussions.

[1] C. Z. Cheng, L. Chen, and M. S. Chance, Ann. Phys. (N.Y.) **161**, 21 (1985).
[2] C. Z. Cheng and M. S. Chance, Phys. Fluids **29**, 3695 (1986).
[3] C. Z. Cheng, Phys. Fluids B **2**, 1427 (1990); C. Z. Cheng, Phys. Fluids B **3**, 2463 (1991).
[4] G. Y. Fu and J. W. Van Dam, Phys. Fluids B **1**, 1949 (1989).
[5] S. von Goeler, W. Stodiek, and N. Sauthoff, Phys. Rev. Lett. **33**, 1201 (1974).
[6] D. J. Campbell *et al.*, Phys. Rev. Lett. **60**, 2148 (1988).
[7] S. Barnabei *et al.*, Phys. Rev. Lett. **84**, 1212 (2000).
[8] C. Z. Cheng and J. R. Johnson, J. Geophys. Res. **104**, 413 (1999).
[9] C. Z. Cheng, J. Geophys. Res. **96**, 21159 (1991).
[10] W. Park *et al.*, Phys. Fluids B **4**, 2033 (1992).
[11] G. Y. Fu and W. Park, Phys. Rev. Lett. **74**, 1594 (1995).
[12] S. Briguglio, G. Vlad, F. Zonca, and C. Kar, Phys. Plasmas **2**, 3711 (1995).
[13] Y. Todo and T. Sato, Phys. Plasmas **5**, 1321 (1998).
[14] C. Z. Cheng, N. N. Gorelenkov, and C. T. Hsu, Nucl. Fusion **35**, 1639 (1995).
[15] N. N. Gorelenkov, C. Z. Cheng, and W. M. Tang, Phys. Plasmas **5**, 3389 (1998).
[16] H. R. Strauss, Phys. Fluids **20**, 1354 (1977).
[17] V. E. Lynch, B. A. Carreras, H. R. Hicks, J. A. Holmes, and L. Garcia, Comput. Phys. Commun. **24**, 465 (1981).
[18] L. A. Charlton, J. A. Holmes, H. R. Hicks, V. E. Lynch, and B. A. Carreras, J. Comput. Phys. **86**, 270 (1990).
[19] Y. Nishimura, J. D. Callen, and C. C. Hegna, Phys. Plasmas **6**, 4685 (1999).
[20] J. A. Holmes *et al.*, Phys. Fluids **25**, 800 (1982).
[21] R. G. Littlejohn, J. Plasma Phys. **29**, 111 (1983).
[22] Originally a fourth order Runge-Kutta-Gill method is employed; See Y. Nishimura *et al.*, Contrib. Plasma Phys. **48**, 224 (2008); Y. Nishimura *et al.*, JAERI-M, 93-140 (1993).
[23] A. M. Dimits and W. W. Lee, J. Comput. Phys. **107**, 309 (1993).
[24] Y. Idomura, S. Tokuda, and Y. Kishimoto, Nucl. Fusion **43**, 234 (2003).
[25] J. Hollenberg and J. D. Callen, Phys. Plasmas **2**, 1917 (1995).